# Controlled One-Dimensional Nanostructures in Poly(3-hexylthiophene) Thin Film for High-Performance Organic Field-Effect Transistors

**Do Hwan Kim, Yunseok Jang, Yeong Don Park, and Kilwon Cho***

*Department of Chemical Engineering, Polymer Research Institute, Pohang University of Science and Technology, Pohang 790-784, Korea*

*Received: May 11, 2006; In Final Form: May 24, 2006*

With the aim of improving the field-effect mobilities in poly(3-hexylthiophene) (P3HT) thin film transistors, we controlled the nanostructures of P3HT thin film by changing the solvent vapor pressure in a spin-coating chamber during solidification. The transistors with P3HT thin films spin-coated under a high solvent vapor pressure (56.5 KPa), showing the one-dimensional nanowire morphologies, resulted in the relatively high field-effect mobilities (0.02 $cm^2/(V \cdot s)$) that are typically more than 1 order of magnitude higher than those prepared under ambient conditions, showing the featureless morphologies. This can be attributed to the higher solvent vapor pressure during film formation, providing the solvent is allowed to evaporate slowly and the degree of ordering within the P3HT crystalline domains is dramatically improved.

## Introduction

Self-organization of $\pi$-conjugated polymers[1−5] on insulator substrates offers a unique strategy for the fabrication of stable, well-defined nanoscale structures that are of potential use as active components in organic field-effect transistors (OFETs).[6−9] In particular, the high field-effect mobility and solution-processability of regioregular poly(3-hexylthiophene) (P3HT) strands have stimulated much interest in their utilization as active electronic elements in various thin film devices and sensors.[10−20] It can be anticipated that the efficiency of charge transport will profit from a better control of structural order with strong $\pi-\pi$ interaction due to one-dimensional (1D) supramolecular self-organization and in turn to higher field-effect mobilities.

Previous work by Ihn et al.[21] has shown that 1D nanofibers of nonregioregular P3HT can be precipitated from bad solvents, and in the study of Kiriy et al.,[22] the tuning of nanofibrils morphology has been achieved by varying the solvent composition (hexane/chloroform). However, in those cases, there was not reported the control of the connectivity of 1D nanofibrils and electrical properties. Especially, in the study by Merlo and Frisbie,[23,24] regioregular P3HT nanofibers have been effectively used in OFETs, and relatively high carrier mobilities have been obtained, but they have not investigated the effect of the dimension, i.e., aspect ratios of the nanofibrils on field-effect mobilities. Further, other fabrication methods for 1D nanowire arrays have been developed, but these generally involve either assemblies of quite complex, amphiphilic block copolymers of conjugated aromatics[25] or relatively complicated experimental procedures such as lithography and Langmuir−Blodgett techniques.[5] Recently, we reported a novel approach for the construction of 1D conjugated P3HT nanowires based on a simple process in which the nanowires with high aspect ratios are spontaneously formed during a simple spin-coating procedure under a high solvent vapor pressure.[26] Further, it was demonstrated that the P3HT chains in nanowires are well-oriented parallel to the insulator substrate.[26,27]

* To whom correspondence should be addressed. E-mail: kwcho@postech.ac.kr.

Here we report on the dependency of the field-effect mobility on aspect ratios and connectivity of the P3HT nanostructures prepared under various solvent vapor pressures. To accomplish that, we fabricated the modified spin-coater with closed chamber, pressure gauge, and heating plate. Therefore, we can easily control the solvent vapor pressure (0−56.5 kPa) by increasing the temperature of the closed chamber with excess solvent. The P3HT thin films were spin-coated on silicon substrates from 0.75 mg/mL solutions in chloroform at 1000 rpm, under various solvent vapor pressures.

## Experimental Section

**Sample Purification.** The regioregular P3HT used in this study was obtained from Rieke Metals Inc. Size exclusion chromatography (SEC) was performed on two mixed bed columns (Polymer Labs PL-mixed C, 300 × 8 mm i.d.), using a tetrahydrofuran eluent (THF, HPLC grade, Duksan), while maintaining the column temperature at 35 °C. The molecular weight ($M_w$ = 54 kg/mol, PDI = 1.8) of P3HT was determined by SEC and calibrated against polystyrene (PS) standards. SEC chromatograms were monitored using a UV/vis detector (Spectra 100, TSP) operating at 400 nm (PS was monitored at 260 nm). To enhance the regioregularity of P3HT, the polymer was purified by continuous extraction with THF and acetonitrile (HPLC grade, Duksan), relying on the solubility difference between the regiorandom and regioregular polymers. The regioregularity (98%) of the as-formed P3HT was estimated from $^1$H NMR by comparing the intensities of the aromatic signals of 7.05, 7.03, 7.00, and 6.98 ppm.

**Sample Preparation.** We fabricated the modified spin-coater with a closed chamber, pressure gauge, and heating plate (Scheme 1). Therefore, we can easily control the solvent vapor pressure by increasing the temperature of the closed chamber with excess solvent. P3HT thin films were spin-coated on silicon substrates from 0.75 mg/mL solutions in chloroform at 1000 rpm, under various solvent vapor pressures. To obtain more precise evidence in nanowire shape (width and length), we observed the transmission electron microscopy (TEM) images

10.1021/jp062899y CCC: $33.50 
Published on Web 07/22/2006

**SCHEME 1: Schematic Representation of the Modified Spin-Coater with Closed Chamber, Pressure Gauge, and Heating Plate**

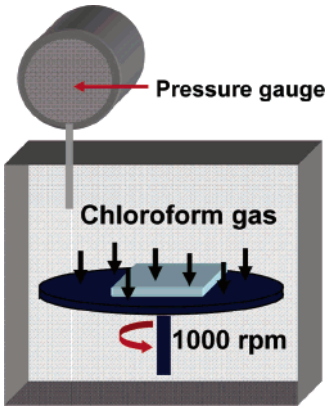


of P3HT films, fabricated under various solvent vapor pressures on a silicon nitride window showing a surface energy similar to that of the silicon ($Si/SiO_2$) system.

**Characterization Techniques.** Morphologies were characterized by scanning force microscopy (Digital Instruments Multimode), operated in the tapping mode using silicon cantilevers with a spring constant of 30 N/m and a tip radius of 13 nm and by transmission electron microscopy (Hitachi-7600), operated at 120 kV. X-ray reflectivity was used to analyze the inner structure of the P3HT nanowires. The measurements were carried out using the bending magnet beam line 3C2 at the Pohang Light Source, Pohang, Korea. X-rays of wavelength $\lambda = 1.5406$ Å monochromatized by a Si(111) double-crystal monochromator were focused at the sample position by a toroidal premirror. NEXAFS spectroscopy was used to determine the conformation of the thienyl backbone chains and the hexyl side chains. These measurements were carried out using the photoemission spectroscopy beam line 2B1 at the Pohang Light Source, Pohang, Korea. The C K-edge NEXAFS spectra were obtained in the total-yield mode with an electrometer (Keithley 617). To investigate the polarization dependence, the incident angle ($\theta$) of the soft X-rays was varied from 20° (electric field vector parallel to the surface normal) to 90° (electric field vector parallel to the surface plane). In addition, the spectra were normalized by the adsorption-edge jump after being divided by that of the $SiO_2$ substrate.

## Results and Discussion

One of the key steps involved in the association of P3HT chains into nanowires is the addition of excess solvent into the modified spin-coating chamber, to give films with thicknesses of about 7−8 nm. This controls the evaporation rate of P3HT solution, which in turn controls the solvent vapor pressure during solidification. To accomplish that, the solvent vapor pressure (0−56.5 kPa) of a chloroform solution of P3HT can be altered simply by changing the amount of solvent and increasing the temperature in the spin-coating chamber.

For samples fabricated under an ambient condition (solvent vapor pressure: 0 kPa), the featureless morphology were observed, as shown in the TEM (Figure 1a) image. Samples prepared from solutions with higher solvent vapor pressures, on the other hand, produced 1D nanorods or nanowires with substantially higher aspect ratios (Figure 1b,c). It might be estimated that some of the nanorods consist of $\pi-\pi$ stacked P3HT chains with limited conjugation length, while the longer nanorods (nanowires) comprise P3HT chains with more extended conjugation length, which may be due to intermolecular rod-to-rod association proposed by the Cacialli group.[26,28,29] It is possible to infer, therefore, that nanowires grow longer as the solvent vapor pressure is increased. Also, it is suspected that the greater solvent vapor pressure (showing more effective solvent annealing rather than lower solvent vapor pressure) inhibits the fast evaporation of the solvent in the P3HT solution, which in turn induces the longer 1D self-assembly without intragrain boundaries (i.e. reduced grain boundaries), governed by the $\pi-\pi$ stacking of P3HT units during solidification, suggesting that the rate of solvent evaporation is one of the critical factors.[30] The rate of solvent evaporation from thin, spin-coated P3HT films could be used to manipulate the growth of 1D nanowires. The morphology of the P3HT films produced by spin-coating under an ambient condition is quite different from the morphology obtained at equilibrium, where the degree of order is low. However, the fabrication of films in high chloroform vapor pressures causes the film to swell, and providing the solvent is allowed to evaporate slowly, the degree of ordering within the crystalline domains is dramatically improved.

In Figure 2 TM-SFM images confirm the formation of P3HT nanowire arrays with well-resolved nanostructures. It is presumed that the solvent-assisted process causes the observed morphological transition in the P3HT system, where the chloroform solvent promotes ordering of the P3HT 1D nanowires within the film during the spin-coating process. Controlling the rate of solvent evaporation induces ordering of the P3HT films at the surface, which then propagates through the entire film (Figure 2b). The solvent imparts mobility to the P3HT chains, enabling a rapid removal of defects such as intragrain boundaries. Thus, highly ordered, nearly defect-free arrays of nanoscopic, 1D nanowires are produced with a high degree of long-range lateral order; i.e., an extension of the 1D nanowires is induced through solvent induced self-assembly. It is clear that the self-assembly of nanowires is governed by $\pi-\pi$ stacking of the regioregular P3HT units. This nanowire morphology with reduced grain boundaries is believed to be the typical signature of the organization of regioregular P3HT strands in the solid state. Also, to clearly elucidate the height and width of P3HT nanowires, P3HT film was spin-coated on silicon substrate from 0.1 mg/mL solution in chloroform at 1000 rpm, under a solvent vapor pressure of 56.5 kPa. The nanowires are in fact ribbonlike objects, as their width is much lager than their height [in the image of Figure 2c,d, the width ranges from 20 to 23 nm, while the height is around 4 nm].

To clearly understand the effect of solvent vapor pressure on morphological transition in P3HT thin film, we conducted the additional experiments such as (1) effect of vapor pressure of argon and not chloroform and (2) effect of temperature and cooling rate of closed chamber during film formation. First, to accomplish that, the argon pressure (0−56.2 kPa) can be altered simply by changing the amount of argon gas in the spin-coating chamber. Figure 3 shows that the featureless morphologies (granular structure) were observed irrespective of argon pressure. Second, to investigate the effect of temperature and cooling rate of the closed chamber on morphological features, we only controlled the temperature in the spin-coating chamber under ambient conditions (solvent vapor pressure: 0 kPa) during film formation. The morphological change was slightly observed for different temperatures of the closed chamber (Figure 4a−d). However, in all cases (40 and 70 °C) nanowires were not observed compared to P3HT film fabricated at 70 °C under a solvent vapor pressure of 56.5 kPa (Figure 4e,f), as shown in

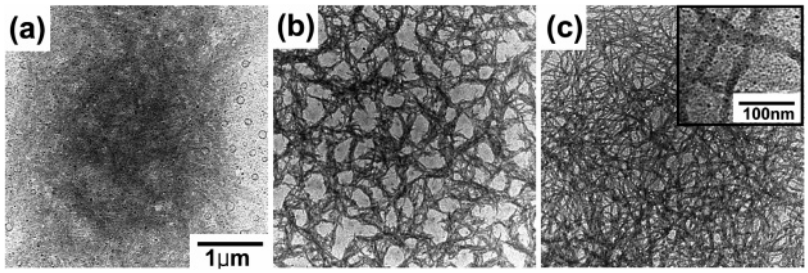


**Figure 1.** Morphological features of spin-coated P3HT films prepared at various solvent vapor pressures with TEM images of P3HT deposited on an insulator substrate under various solvent vapor pressures: (a) ambient; (b) 36.5 kPa; (c) 56.5 kPa.

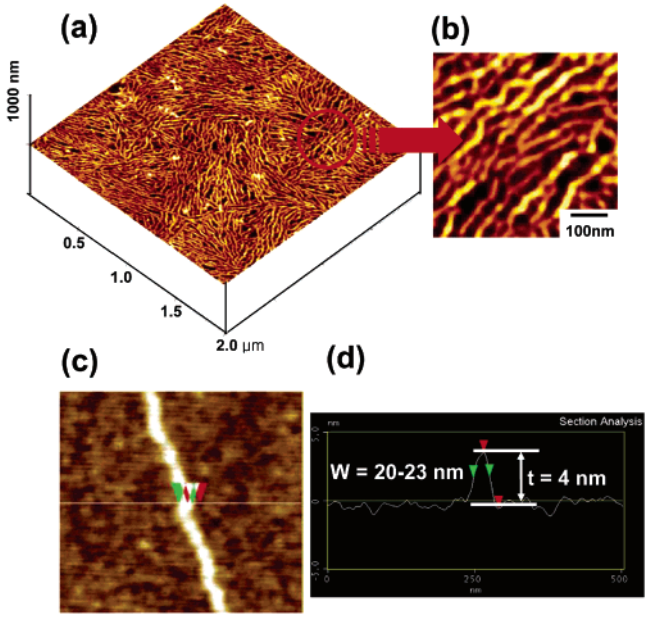


**Figure 2.** Morphological features of spin-coated P3HT films prepared at 56.5 kPa: (a) low ($2 \times 2\ \mu m^2$) and (b) high magnified ($500 \times 500$ $nm^2$) images of tapping mode scanning force microscopy (TM-SFM); (c) morphological feature and (d) height profile of P3HT single nanowire spin-coated on a silicon substrate from 0.1 mg/mL solution in chloroform at 1000 rpm, under a solvent vapor pressure of 56.5 kPa (thickness ($t$) $\sim$ 4 nm and width ($w$) $\sim$ 20 nm).

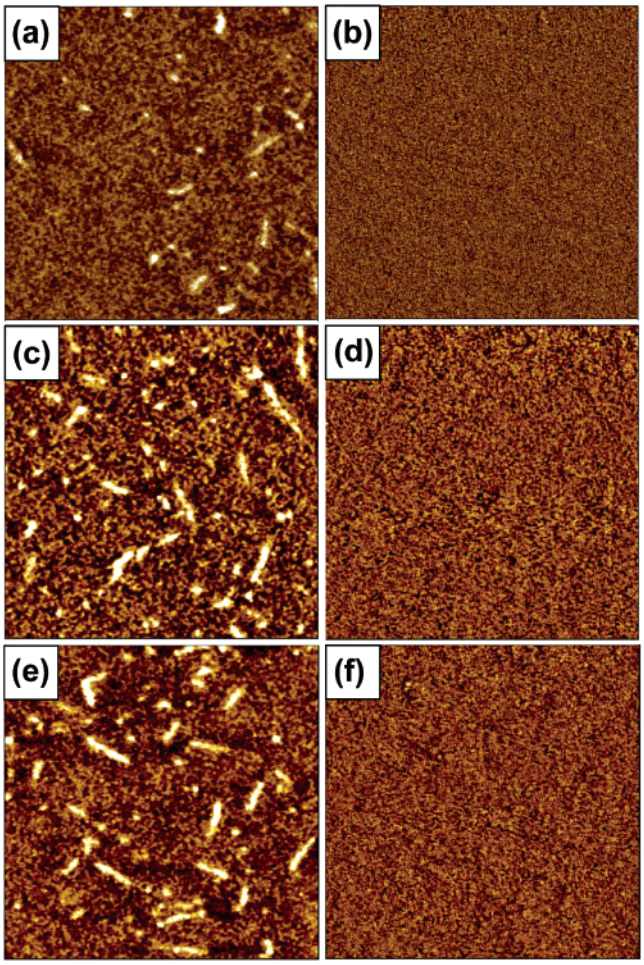


**Figure 3.** TM-SFM images of spin-coated P3HT films prepared at various argon pressures: ambient [(a) topography and (b) phase]; 33.4 kPa [(c) topography and (d) phase]; 56.2 kPa [(e) topography and (f) phase].

the TM-SFM images. From these results, we can conclude that vapor pressure and temperature do not induce the morphological transition during solidification. That is, the fabrication of P3HT films in high chloroform vapor pressures causes the film to swell, and providing the solvent is allowed to evaporate slowly, the morphological transition can be obtained. Only in chloroform solvent vapor, the P3HT molecules have the evident proclivity to self-assemble into definite, extension-forming nanowire-like assemblies, with well-defined widths and heights.

The inner structures of the P3HT thin film with solvent vapor pressures were analyzed using synchrotron X-ray reflectivity as shown in Figure 5. The measurements were carried out using the bending magnet beam line 3C2 at the Pohang Light Source. X-rays of wavelength $\lambda = 1.5406$ Å monochromatized by a Si(111) double-crystal monochromator were focused at the sample position by a toroidal premirror. Both Kiessig fringes, caused by interference of beams reflected at the air−polymer and polymer−substrate interfaces, and Bragg peaks are observed in the reflectivity pattern of the P3HT thin films. The total thickness of the film ($\sim$50 Å) can be derived from the distance between the subsequent maxima of the Kiessig fringes, which are modulated by Bragg peaks. Bragg peaks (indicated by arrows) are caused by a periodic density modulation perpendicular to the surface and are taken as representative of the as-formed ordered phase. The P3HT layer thickness was thus determined to be approximately 17.7 Å (ambient condition $\sim$ 0 kPa) and 18.2 Å (56.5 kPa). This difference in the P3HT layer thickness according to solvent vapor pressure is not fully understood. However, these values are approximately double the extended length of the side chain ($\sim$8 Å), as calculated by summing over the atom−atom distances in the side chain, indicating that the P3HT thin films adopt a bilayer structure irrespective of solvent vapor pressures, as depicted in Figure 5. However, it is difficult to characterize the structure of the region close to the substrate using X-ray reflectivity.

NEXAFS spectroscopy is a powerful tool for the determination of molecular orientation at the surface. In this study, NEXAFS has been employed to elucidate the conformation of P3HT chains in nanowires. Figure 6 shows a series of NEXAFS

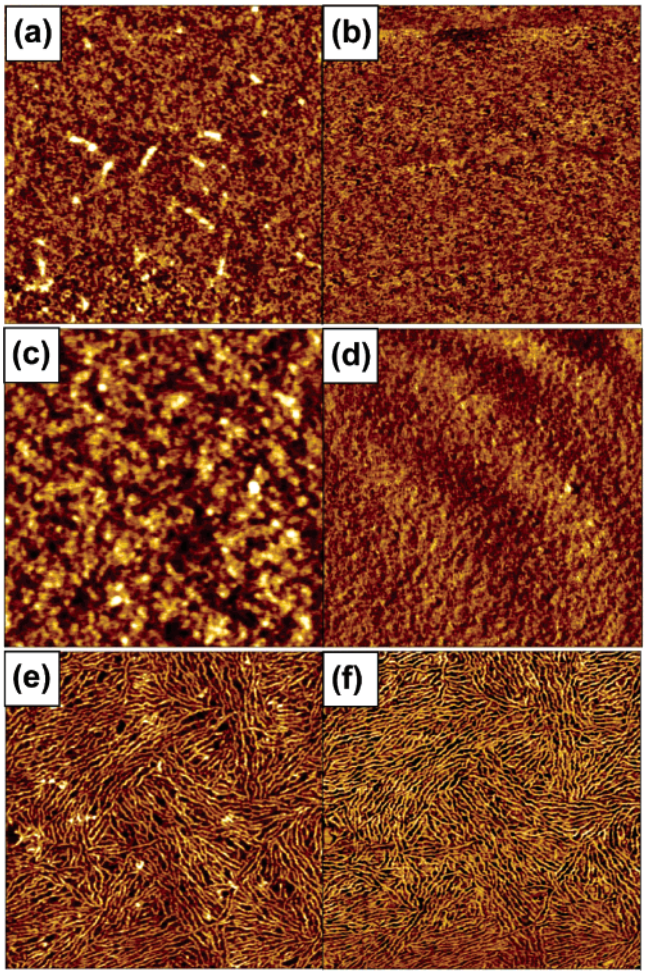


**Figure 4.** TM-SFM images of spin-coated P3HT films prepared at various temperatures of a closed chamber: 40 °C [(a) topography and (b) phase] and 70 °C [(c) topography and (d) phase] under ambient conditions; 70 °C [(e) topography and (f) phase] under a solvent vapor pressure of 56.5 kPa.

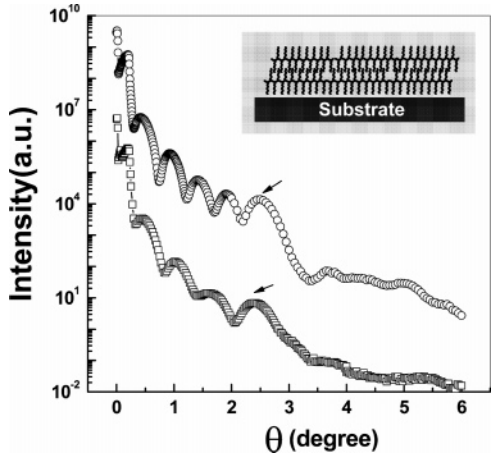


**Figure 5.** Synchrotron X-ray reflectivity patterns showing the inner structure in P3HT thin film grown on insulator substrates: ○, ambient condition (0 kPa); □, 56.5 kPa. The inset reveals a schematic representation of the internal structure of P3HT thin film.

spectra obtained at two different incident angles, 90 and 20° at room temperature. The spectra are dominated by four resonances, originating from the C−H/Rydberg, C−C $\sigma$* orbitals, C═C $\sigma$* orbitals, and C═C $\pi$* orbitals. The sharp features situated at 288.1 and 285.5 eV originate from transitions into several Rydberg states, with dipole transition moments lying

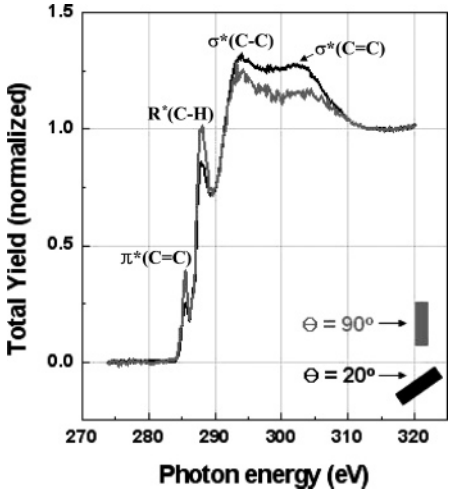


**Figure 6.** NEXAFS spectra of the C 1s edge of P3HT 1D nanowires deposited on an insulator substrate recorded for different angles of incidence ($\theta$) of incoming photons.

in the plane of the C−H valance orbitals and transitions into C═C $\pi$* orbitals.[30−33] The intensities of these components at normal X-ray incidence ($\theta$ = 90°) are stronger than those obtained at grazing incidence ($\theta$ = 20°). The broader resonances at around 293.5 and 303.7 eV can be assigned to transitions into the C−C $\sigma$* orbital and C═C $\sigma$* orbitals, respectively.[33,34] The intensity at grazing X-ray incidence is stronger than that at normal incidence. The transitions into the C−H/Rydberg and C−C $\sigma$* orbitals show an opposite polarization dependence with changing incident angle. These results demonstrate that the side chains in the surface layer are oriented almost perpendicularly to the surface,[11,20] in which the $CH_3$ groups are exposed at the surface. Moreover, the backbone (thienyl group) chains in P3HT 1D nanowires are oriented parallel to the insulator substrate, demonstrating an opposite polarization dependence with changing incident angle for transitions into C═C $\pi$* orbitals and C═C $\sigma$* orbitals.

With the aim of determining the relationship between field-effect mobility and morphological feature, the mobilities of regioregular P3HT were measured by using a top-contact, thin film field-effect transistor (FET). A cross-sectional view of the transistor device is shown in Figure 7a. A 300 nm thick silicon oxide gate dielectric (capacitance = 10.8 nF $cm^{-2}$) was thermally grown on a highly doped silicon wafer. P3HT thin films were then spin coated from 0.75 mg/mL solutions in chloroform at 1000 rpm, under various solvent vapor pressures. Finally, the source and drain electrodes of 70 nm Au were evaporated onto the P3HT thin film surface through a shadow mask, at a slow rate under vacuum. The as-formed transistors had a channel width of 400 $\mu$m and a channel length of 40 $\mu$m.

Figure 7a shows typical drain current ($I_{DS}$) vs source-drain voltage ($V_{DS}$) plots obtained at various gate voltages, for P3HT film with nanowire-like morphologies. Table 1 shows the variations in the field-effect mobility according to solvent vapor pressure, obtained by plotting the square root of the drain current vs gate voltage ($V_{DS}$ = −80 V), as shown in Figure 7c. The results show that samples fabricated under high solvent vapor pressures (displaying nanowires in P3HT film) produce field-effect mobilities ($\sim 1.4 \times 10^{-2}$ $cm^2$ $V^{-1}$ $s^{-1}$) that are more than 1 order of magnitude higher than those of samples ($\sim 1.2 \times 10^{-3}$ $cm^2$ $V^{-1}$ $s^{-1}$) prepared under an ambient condition (0 kPa). Also, from Figure 7b and Table 1 it can be observed that samples fabricated under high solvent vapor pressures represent the higher on/off ratio ($\sim 10^4$) and lower threshold voltage ($V_{th}$

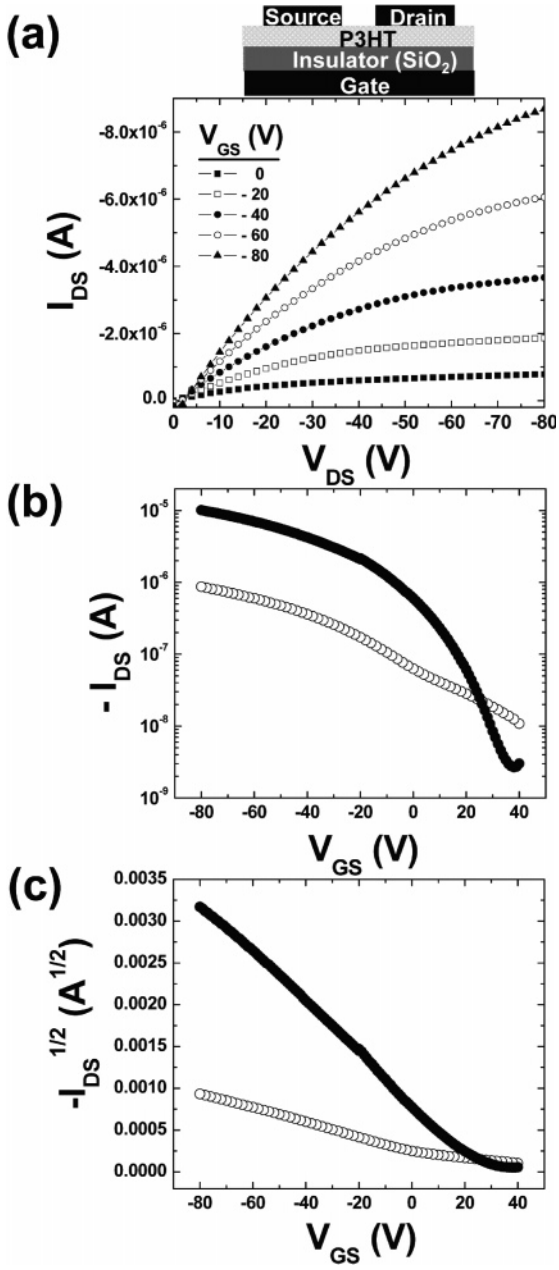


**Figure 7.** (a) Current−voltage characteristics of a 40 (long) by 400 (wide) $\mu$m transistor fabricated under high solvent vapor pressure of ~56.5 kPa (displaying the 1D nanowires). The schematic inset in (a) depicts the device structure used in the current investigation. Transfer characteristics are (b) [$-I_{DS}$ vs $V_{GS}$ at $V_{DS} = -80$ V] and (c) [$(-I_{DS})^{1/2}$ vs $V_{GS}$ at $V_{DS} = -80$ V] with respect to solvent vapor pressure (○, ambient; ●, 56.5 kPa).

**TABLE 1: Average Mobility, $V_{th}$, and On/Off Ratio Values Obtained from the Transfer Curve of the P3HT FETs According to Various Solvent Vapor Pressures**

| solvent vapor pressure (kPa) | on/off ratio | $V_{th}$ (V) | av mobility, $\mu$ ($cm^2\ V^{-1}\ s^{-1}$) |
|---|---|---|---|
| 0 (ambient) | $\sim 10^2$ | 34 | $(1.2 \pm 0.3) \times 10^{-3}$ |
| 36.5 | $\sim 10^2$ | 40 | $(4.2 \pm 0.3) \times 10^{-3}$ |
| 42.7 | $\sim 10^3$ | 37 | $(6.9 \pm 0.5) \times 10^{-3}$ |
| 48.9 | $\sim 10^4$ | 28 | $(1.3 \pm 0.5) \times 10^{-2}$ |
| 56.5 | $\sim 10^4$ | 25 | $(1.4 \pm 0.2) \times 10^{-2}$ |

~ 25 V) rather than those (on/off ratio ~ $10^2$, $V_{th}$ ~ 34 V) of sample fabricated under ambient conditions. This surprising increase in the field-effect mobility and on/off modulation might be attributed to the 1D nanowire morphology. In the nanowire system of P3HT, the mobility obtained in our experiments is lower than that in the work of Frisbie.[23,24] In our case, we fabricated the TFT devices with a channel length of 40 $\mu$m and a width of 400 $\mu$m and measured the transfer characteristics under nitrogen conditions unlike the devices fabricated by Frisbie (channel length ~ 1 $\mu$m, under vacuum). Therefore, it is difficult to compare the two cases directly. Also, in our case, the P3HT film was totally coated on the insulator substrate. In other words, the part without nanowires is not bare insulator surface but coated P3HT film not containing one-dimensional nanorods or nanowires. Therefore, in the mobility determination between electrodes, we just used the channel dimension. Well-ordered structure of these 1D nanowires enables the charge carrier to transport in a two-dimensional conjugation direction,[35] i.e., through $\pi-\pi$ overlapping, resulting in high field-effect mobilities. Therefore, we can conclude that the striking change in the field-effect mobility, caused by the different morphological features of the nanocrystallite, is clear evidence that the effects of this ordering dominate the transport.

## Conclusion

In summary, we could control the nanomorphology and field-effect mobility by changing the solvent vapor pressure during the solidification of spin-coated P3HT thin films for high-performance organic transistors. Samples fabricated under a high solvent vapor pressure (nanowire morphology) resulted in the occurrence of field-effect mobilities that are typically more than 1 order of magnitude higher than those of samples prepared under an ambient condition (featureless morphology).

**Acknowledgment.** This work was supported by the National Research Laboratory Program and ERC Program (Grant R11-2003-006-03005-0) of the MOST/KOSEF, Grant F0004022 from the Information Display R&D Center under the 21st Century Frontier R&D Program and the Regional Technology Innovation Program (RT104-01-04) of the Ministry of Commerce, Industry, and Energy of Korea, and the BK21 Program of the Ministry of Education and Human Resources Development of Korea and the Pohang Acceleratory Laboratory, providing the synchrotron radiation source at the 2B1, 4B1, 3C2, 4C2, and 8C1 beam lines used in this study.

## References and Notes

(1) Liang, L.; Liu, J.; Windisch, C. F.; Exarhos, G. J.; Lin, Y. *Angew. Chem., Int. Ed.* **2002**, *41*, 3665.
(2) Samorì, P.; Francke, V.; Müllen, K.; Rabe, J. P. *Chem.—Eur. J.* **1999**, *5*, 2312.
(3) Maynor, B. W.; Filocamo, S. F.; Grinstaff, M. W.; Liu, J. *J. Am. Chem. Soc.* **2002**, *124*, 522.
(4) Carswell, A. D. W.; ÕRear, E. A.; Grady, B. P. *J. Am. Chem. Soc.* **2003**, *125*, 14793.
(5) Bjørnholm, T.; Hassenkam, T.; Greve, D. R.; McCullough, R. D.; Jayaraman, M.; Savoy, S. H.; Jones, C. E.; McDevitt, J. T. *Adv. Mater.* **1999**, *11*, 1218.
(6) Bao, Z.; Dodabalapur, A.; Lovinger, A. J. *Appl. Phys. Lett.* **1996**, *69*, 4108.
(7) Sirringhaus, H.; Tessler, N.; Friend, R. H. *Science* **1998**, *280*, 1741.
(8) Sirringhaus, H. *Adv. Mater.* **2005**, *17*, 2411.
(9) Yoon, M.-H.; Yan, H.; Facchetti, A.; Marks, T. J. *J. Am. Chem. Soc.* **2005**, *127*, 10388.
(10) Österbacka, R.; An, C. P.; Jiang, X. M.; Vardeny, Z. V. *Science* **2000**, *287*, 839.
(11) Sirringhaus, H.; Brown, P. J.; Friend, R. H.; Nielsen, M. M.; Bechgaard, K.; Langeveld-Voss, B. M. W.; Spiering, A. J. H.; Janssen, R. A. J.; Meijer, E. W.; Herwig, P.; de Leeuw, D. M. *Nature* **1999**, *401*, 685.
(12) Dodabalapur, A. *Appl. Phys. Lett.* **1998**, *73*, 142.
(13) Dimitrakopoulos, C. D.; Malenfant, P. R. L. *Adv. Mater.* **2002**, *14*, 99.
(14) Kline, R. J.; McGehee, M. D.; Kadnikova, E. N.; Liu, J.; Fréchet, J. M. J. *Adv. Mater.* **2003**, *15*, 1519.

(15) Mas-Torrent, M.; den Boer, D.; Durkut, M.; Hadley, P.; Schenning, A. P. H. J. *Nanotechnology* **2004**, *15*, S265.

(16) Kim, D. H.; Park, Y. D.; Jang, Y.; Yang, H.; Kim, Y. H.; Han, J. I.; Moon, D. G.; Park, S.; Chang, T.; Chang, C.; Joo, M.; Ryu, C. Y.; Cho, K. *Adv. Funct. Mater*. **2005**, *15*, 77.

(17) Kim, D. H.; Jang, Y.; Park, Y. D.; Cho, K. *Langmuir* **2005**, *21*, 3203.

(18) Chang, J.-F.; Sun, B.; Breiby, D. W.; Nielsen, M. M.; Soelling, T. I.; Giles, M.; McCulloch, I.; Sirringhaus, H. *Chem. Mater*. **2004**, *16*, 4772.

(19) Babel, A.; Jenekhe, S. A. *Macromolecules* **2004**, *37*, 9835.

(20) Kline, R. J.; McGehee, M. D.; Kadnikova, E. N.; Liu, J.; Frećhet, J. M. J.; Toney, M. F. *Macromolecules* **2005**, *38*, 3312.

(21) Ihn, K. J.; Moulton, J.; Smith, P. *J. Polym. Sci., Part B: Polym. Phys*. **1993**, *31*, 735.

(22) Kiriy, N.; Jähne, E.; Alder, H.; Schneider, M.; Kiriy, A.; Gorodyska, G.; Minko, S.; Jehnichen, D.; Simon, P.; Fokin, A. A.; Stamm, M. *Nano Lett*. **2003**, *3*, 707.

(23) Merlo, J. A.; Frisbie, C. D. *J. Polym. Sci., Part B: Polym. Phys*. **2003**, *41*, 2674.

(24) Merlo, J. A.; Frisbie, C. D. *J. Phys. Chem. B* **2004**, *108*, 19169.

(25) Liu, J.; Sheina, E.; Kowalewski, T.; McCullough, R. D. *Angew. Chem., Int. Ed.* **2002**, *41*, 329.

(26) Kim, D. H.; Park, Y. D.; Jang, Y.; Kim, S.; Cho, K. *Macromol. Rapid Commun*. **2005**, *26*, 834.

(27) Yang, H.; Shin, T. J.; Yang, L.; Cho, K.; Ryu, C. Y.; Bao, Z. *Adv. Funct. Mater*. **2005**, *15*, 671.

(28) Cacialli, F.; Wilson, J. S.; Michels, J. J.; Daniel, C.; Silva, C.; Friend, R. H.; Severin, N.; Samorì, P.; Rabe, J. P.; O'Connell, M. J.; Taylor, P. N.; Anderson, H. L. *Nat. Mater*. **2002**, *1*, 160.

(29) Liu, H.; Wang, S.; Luo, Y.; Tang, W.; Yu, C.; Li, L.; Chen, C.; Liu, Y.; Xi, F. *J. Mater. Chem*. **2001**, *11*, 3063.

(30) Kim, S. H.; Misner, M. J.; Xu, T.; Kimura, M.; Russell, T. P. *Adv. Mater*. **2004**, *16*, 226.

(31) Bagus, P. S.; Weiss, K.; Schertel, A.; Wöll, Ch.; Braun, W.; Hellwig, C.; Jung, C. *Chem. Phys. Lett*. **1996**, *248*, 129.

(32) Weiss, K.; Bagus, P. S.; Wöll, Ch. *J. Chem. Phys*. **1999**, *111*, 6834.

(33) Tourillon, G.; Fontaine, A.; Garrett, R.; Sagurton, M.; Xu, P.; Williams, G. P. *Phys. Rev. B* **1987**, *35*, 9863.

(34) Outka, D. A.; Stöhr, J.; Rabe, J. P.; Swalen, J. D. *J. Chem. Phys.* **1988**, *88*, 4076.

(35) Dicker, G.; de Haas, M. P.; Warman, J. M.; de Leeuw, D. M.; Siebbeles, L. D. A. *J. Phys. Chem. B* **2004**, *108*, 17818.